Hindawi Publishing Corporation
Journal of Nanomaterials
Volume 2012, Article ID 612420, 9 pages
doi:10.1155/2012/612420

Research Article

Gas Sensing Properties and Mechanism of Nano-SnO_2-Based Sensor for Hydrogen and Carbon Monoxide

Weigen Chen, Qu Zhou, Fu Wan, and Tuoyu Gao

State Key Laboratory of Power Transmission Equipment & System Security and New Technology, Chongqing University, Chongqing 400030, China

Correspondence should be addressed to Qu Zhou, zhouqupsd@yahoo.cn

Received 17 September 2012; Revised 27 October 2012; Accepted 4 November 2012

Academic Editor: Wen Zeng

Nano-SnO_2 powder was prepared by the hydrothermal method in this paper. X-ray powder diffraction (XRD) and scanning electron microscopy (SEM) were used to characterize the composition of the crystalline phase and the morphology of the prepared gas-sensitive materials, respectively. In particular, the study focused on the sensing behaviors of nano-SnO_2-based sensor towards power transformer fault gases such as hydrogen and carbon monoxide. The optimum working temperature for hydrogen and carbon monoxide is about 400°C and 360°C, separately. Further investigations into the adsorption process of gas molecule on SnO_2 (110) surface based on the first principles were conducted. The calculations indicated that 1σ orbits of H_2 split into several new electronic peaks and 5σ orbits of CO almost degenerated completely in the adsorption process, which promoted charge transfer between gas molecule and SnO_2 (110) surface. It provides a qualitative explanation for the prepared nano-SnO_2-based sensor exhibiting different gas sensing properties towards H_2 and CO.

1. Introduction

Power transformer is one of the most important apparatus in power transmission. The safety and reliability of the power system are directly affected by the operation conditions. Once faults happen on power transformer, it will cause great damage to the national economy [1–4]. At present, most of the large power transformers are still oil-immersed transformers, when the transformer internal paper-oil insulation faults occur due to overheating or partial discharge [2, 3], they may cause gaseous compounds such as hydrogen, carbon oxides, and some low molecular hydrocarbons, and most of those fault gases would dissolve in transformer oil [5–8]. Dissolved gas-in-oil analysis (DGA) and online monitoring of the dissolved gases in transformer oil are two important technologies for power transformer conditional maintenance.

At present, we mainly use gas chromatography, flourier transform infrared spectroscopy, Raman spectrometry, and photoacoustic spectrometry to detect the dissolved gases in transformer oil. With the development of nanotechnology, there is a new trend to use gas sensor based on nanometric materials detecting the dissolved gases. With many advantages such as simple manufacture technique, low cost, rapid response and recovery time, and long life and stability, semiconductor metal oxides such as SnO_2 is promising for online monitoring the fault gases in power transformer [9–16]. However, due to the similar element compositions and molecular structures of transformer fault gases, it is difficult to understand the sensing behaviors of SnO_2 to those gases [17, 18]. Although many relevant researches have been carried out, an atomic level understanding of SnO_2-based materials sensing properties toward transformer fault gases is crucial [19–22]. As both H_2 and CO are the effective fault gases in power transformers, the sensing properties of nano-SnO_2-based gas sensor to H_2 and CO were investigated in this paper.

In this paper, the nano-SnO_2 sensing materials were prepared by the hydrothermal method; its microstructure and gas sensing properties towards H_2 and CO were investigated. Furthermore, an atomic level understanding of the sensing properties based on the first principles calculations

was carried out. The main purpose is to make clear the gas response properties of nano-SnO_2 towards H_2 and CO. This study promises a new feasible way to explore new gas sensors for the on-line monitoring of fault gases dissolved in power transformers.

2. Experiment Process

2.1. Synthesis of Nano-SnO_2 Sensing Materials. Nano-SnO_2 powder was synthesized via hydrothermal method. Firstly, 1.753 g $SnCl_4 \cdot 5H_2O$ (A.R.) was dissolved in a beaker with 20 mL deionized water and 20 mL absolute ethanol; $NH_3 \cdot H_2O$ (A.R.) was dropped into the mixed solution until the pH reached 9 under intense magnetic stirring. After magnetic stirring for about 30 min at 70°C, the mixture solution was transferred into a Teflon-lined autoclave with capacity of 50 mL, which was heated at 180°C for 24 h. Then the autoclave was cooled at room temperature naturally. Finally, the as-obtained powder was washed with deionized water and ethanol several times, respectively, until Cl^- could not be examined by 0.1 mol/L $AgNO_3$ aqueous solution and dried in air for the further characterizations.

2.2. Fabrication of Nano-SnO_2 Gas Sensor. Nano-SnO_2 based gas sensor was fabricated through traditional side heating preparation process. The powder was mixed with diethanolamine and ethanol to obtain a homogenous paste. It was subsequently brushed onto an alumina tube substrate, and dried at 100°C for 2 h in air. Then, a Ni-Cr heating wire was inserted into the alumina tube substrate. Finally, the tube was welded on the pedestal of the sensor. Figure 1(a) shows the schematic drawing of the as-fabricated gas sensor. As illustrated in Figure 1(b), there are Au electrodes placed at the two sides of the alumina tube to read the electrical resistance of gas sensor. The distance between the two electrodes is estimated to be 6 mm, and the diameter of the tube is 1.2 mm. Then the gas sensor is aged at 120°C for 240 h to improve its stability and repeatability.

2.3. Characterization of Structure and Gas Sensing Property. X-ray powder diffraction (XRD) was taken to identify the crystalline phase composition of the prepared nano-SnO_2 samples at the range of 20–80° with Cu $K_{\alpha 1}$ radiation (λ = 1.5406 Å) at 40 kV and 40 mA. The morphology of SnO_2 nanostructures was characterized by scanning electron microscopy (SEM).

The static measuring system was used to test gas sensing properties. The operating temperature of the gas sensor was controlled by varying the current of Ni-Cr heating wire. Gas sensing properties were studied under laboratory condition with room temperature at 30°C and humidity as 50%. The relative variation of the gas sensor resistance (gas response) in this paper was defined as $S = (R_o - R)/R_o$, where R_o and R represent the resistances of the sensor in N_2 and in targeted gas, respectively. All measurements were repeated several times in order to ensure the reproducibility of the gas sensing response.

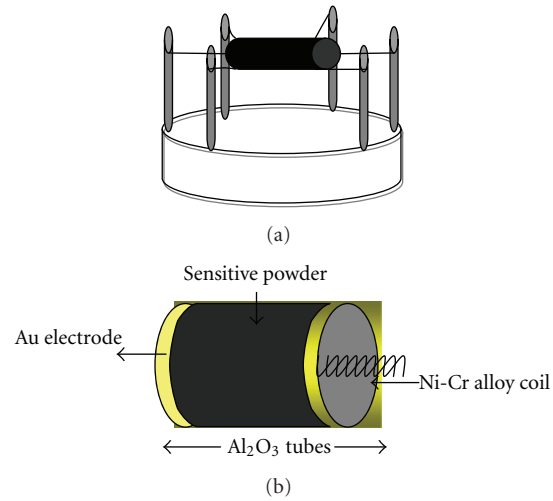

Figure 1: The structure of gas sensor ((a) base structure; (b) tube structure).

2.4. First Principles Calculation. Based on the density functional theory (DFT) [23–25], the first principles calculations were performed with the assistant of Cambridge Sequential Total Energy Package (CASTEP) program in this paper [26, 27]. Exchange-correlation function between electrons was described by the Revised Perdew-Burke-Ernzerhof (RPBE) form of generalized gradient approximation (GGA). Interaction between nuclei and electrons was approximated with ultrasoft pseudopotential to treat the valence electrons, and the valence electron configurations for H, C, O, and Sn atoms were chosen as 1s, 2s 2p, 2s 2p, and 5s 5p, respectively. The cutoff energy of the plane-wave was set at 380 eV to ensure energy convergence within 1-2 meV/atom. The maximum root mean square convergent tolerance was 1.0×10^{-6} eV/atom. In the whole process of geometry optimization and energy calculation, all atoms were allowed to relax in all directions freely [28–31].

3. Results and Discussion

3.1. Characteristic of Sensing Material. To determine the crystalline phase composition of the prepared SnO_2 powder, the X-ray diffraction pattern of the sample is shown in Figure 2. One can clearly see that the main characteristic peaks (110), (101), and (211) appeared in 27.9°, 34.3°, and 52.4° respectively, perfectly corresponding to the tetragonal rutile phase of SnO_2 with the lattice constants of a = 4.738 Å and c = 3.188 Å (JCPDS21-1250). The average particle size of the sample is calculated from the XRD peaks based on the Scherer formula as follows:

$$D = \frac{0.89\gamma}{(\beta \cos\theta)}, \quad (1)$$

where D is the mean particle size of the powder, γ is the X-ray wavelength, β is the half peak width, and θ is the Bragg angle. According to the broadening of the (110) diffraction line, the calculated average particle size is about 20 nm.

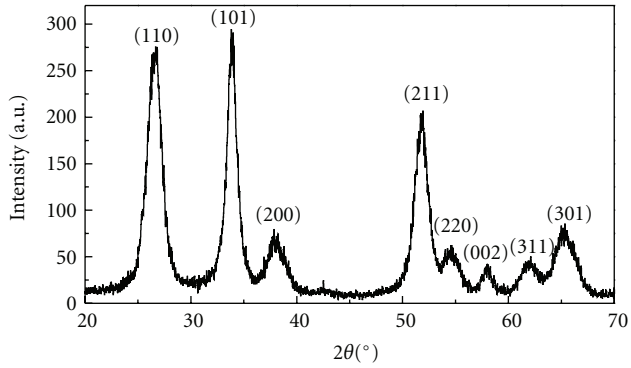

Figure 2: XRD spectra of the nano-SnO_2 powder.

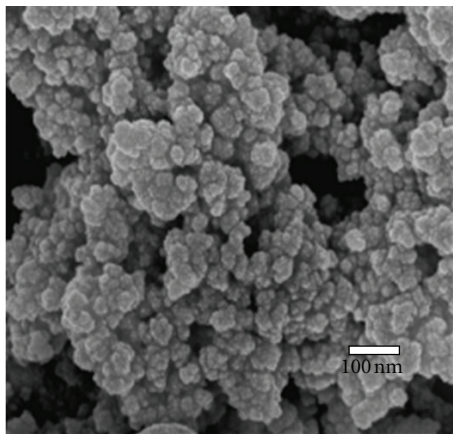

Figure 3: EM micrograph of the nano-SnO_2 powder.

Figure 3 shows the SEM image of the prepared nano-SnO_2 sample, which is disperse, and the particles are uniform in shape and particle size. They are nearly spherical with the diameters about 25–30 nm.

3.2. Gas Sensing Properties

3.2.1. Optimum Operating Temperature Property. The operating temperature is one of the most important properties of the as-prepared gas sensor. The optimum operating temperature is closely related to not only nature property of the material itself, but also the gas-sensing process of the gas towards the surface of materials. To investigate the operating temperature property of the prepared nano-SnO_2-based gas sensor, the gas response to transformer fault gases at different temperatures was measured.

Figure 4 shows the response of nano-SnO_2-based gas sensor to hydrogen and carbon monoxide as a function of the operating temperature, with the gas concentration as 50 ul/L, environmental temperature at 30°C and humidity as 50%. As shown in Figure 4, the gas responses increase firstly and then decrease with the rise of operating temperature, which can be explained by a dynamic equilibrium state of adsorption and desorption. With the operating temperature increasing, the adsorption amount of the gas would reach to a balance

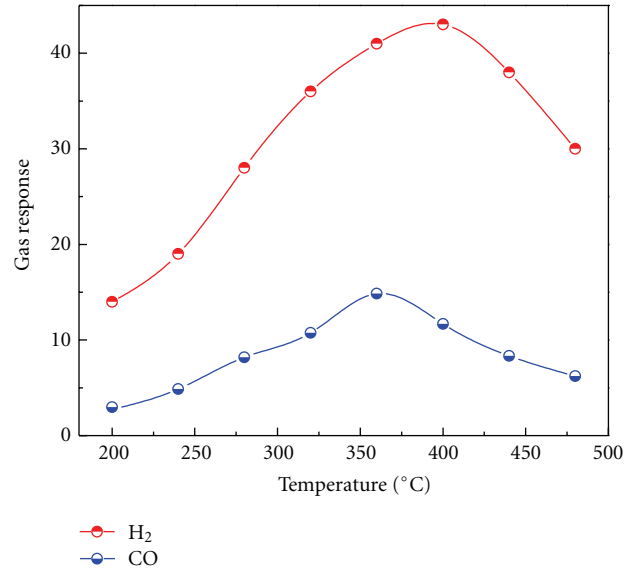

Figure 4: Gas response of the sensor to different operating temperatures.

at a suitable temperature firstly. And then the balance of desorption is broken which is followed by the decrease of gas response. The gas response to 50 ul/L hydrogen and carbon monoxide at different operating temperatures can be seen clearly from Figure 4. The optimum operating temperature for carbon monoxide and hydrogen are revealed to be about 360°C and 400°C, respectively, indicating that the sensor shows the maximum gas response at these temperatures.

3.2.2. Gas Response Property. If gas response of the prepared gas sensor presents a linear or quasilinear relationship with the concentration of the measured gas, the gas sensor can be used in the on-line monitoring of the fault gases dissolved in power transformer oil. The gas sensor responses were tested with the concentration of the target gas in the range of 5–100 ul/L, environmental temperature at 30°C, and humidity as 50%.

Figure 5 shows the gas response to hydrogen and carbon monoxide as a function of the gas concentration at their optimum operating temperatures. From Figure 5, it can be demonstrated that the gas responses have the trend of increasing at different degrees with rising of gas concentration. The gas response curves meet the quasi-linear relationship with the concentrations of the detected gases, satisfying the requirements of engineering application for on-line monitoring.

3.2.3. Response-Recovery Property. The response time and recovery time are the other two key properties for gas sensor, which are defined as the required time for reaching 90% of the maximum response when gas in and 10% when gas out, respectively. Figure 6 shows the response-recovery property of the sensor working at their optimum operating temperatures, with gas concentration of 50 ul/L, environmental temperature at 30°C and humidity as 40%. From the curves,

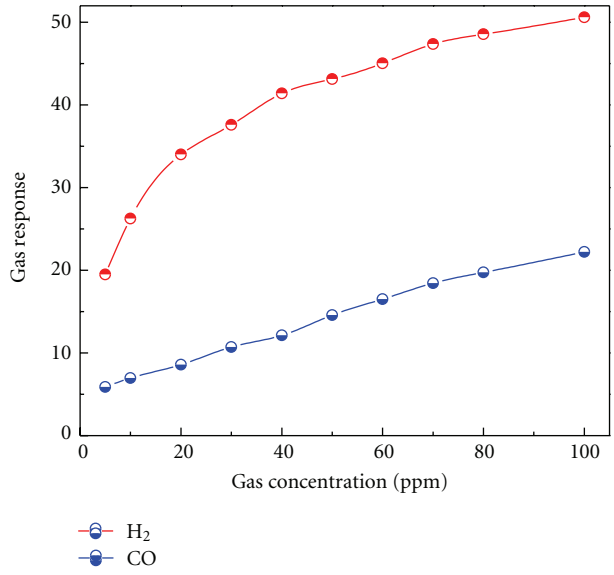

Figure 5: Gas response of the sensor to different gas concentrations.

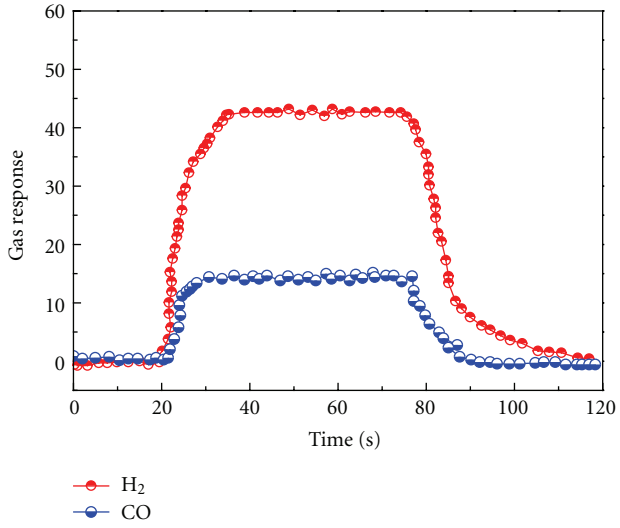

Figure 6: Response and recovery time of the gas sensor.

it can be known that the gas response increases sharply with gas in and returns to its original state while gas out. According to the definition above, the response and recovery time for hydrogen as shown in Figure 6 is about 12 s and 25 s, for carbon monoxide about 8 s and 15 s, respectively.

3.2.4. Stability and Repeatability. Finally, the stability of the sensor to 50 ul/L fault gases was investigated with their optimum operating temperatures, environmental temperature at 30°C, and humidity as 40%. As shown in Figure 7, the gas response changes slightly for two months, which indicates that the prepared gas sensor presents excellent long-term stability and repeatability.

3.3. Gas Sensing Mechanism. According to the researches above, it can be concluded that even at the same experiment

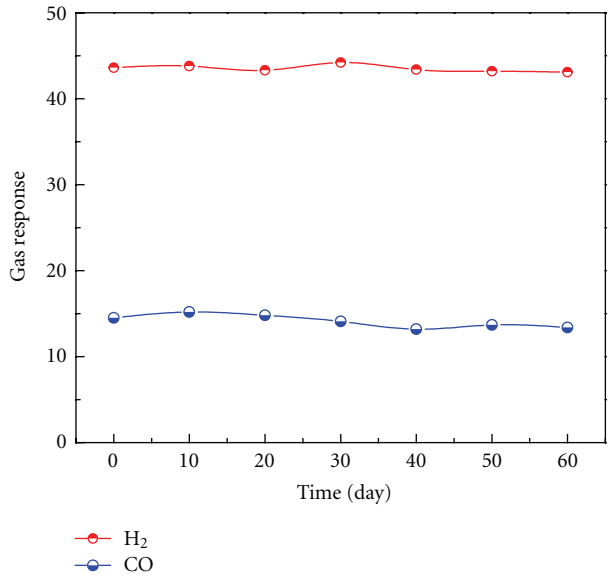

Figure 7: The long-term stability and repeatability of the sensor.

conditions, the prepared gas sensor exhibits different sensing properties such as the optimum operating temperature property and gas response property. The previous studies about gas sensing mechanism mainly concentrated on the grain size [33], grain growth direction [34], specific surface area [35–38], and so forth. But they could not have given a reasonable explanation for sensing variances of gas sensor to different gases [39]. So it is needed to further study the gas sensing reaction process in atomic level to figure out more accurate mechanism [40–42].

At present researchers mainly consider the sensing behaviors of semiconductor metal oxides through a trial-and-error experiment method, which wastes a lot of unnecessary manpower, materials, finance, and time [43]. With the development of computer technology, they can be studied by theoretical calculation method. Although many works have been conducted on nano-SnO_2-based sensor, its gas sensing mechanism remains controversial.

SnO_2 is a typical n-type semiconductor as reported, and its gas sensing property was mainly determined by the surface. When placed in a gas with certain concentration, it would be adsorbed by gas molecule on its surface firstly, and then the resistance and conductance of the surface would be modified. In order to reveal the different gas responses against hydrogen and carbon monoxide, the adsorption process between the gas molecule and sensing surface should be investigated deeply to gain an insight into the gas sensing mechanism.

It is well known that the sensing property of SnO_2 is dominantly controlled by surface, and that SnO_2 crystal has four major low-index surfaces (110), (101), (100), and (001) [23, 38], respectively. In particular, the (110) surface is of the most thermodynamically stable surface among the four low-index surfaces [19, 26, 27], and it has been widely used to investigate the surface properties of SnO_2 through the first principles method. To understand the sensing mechanism of

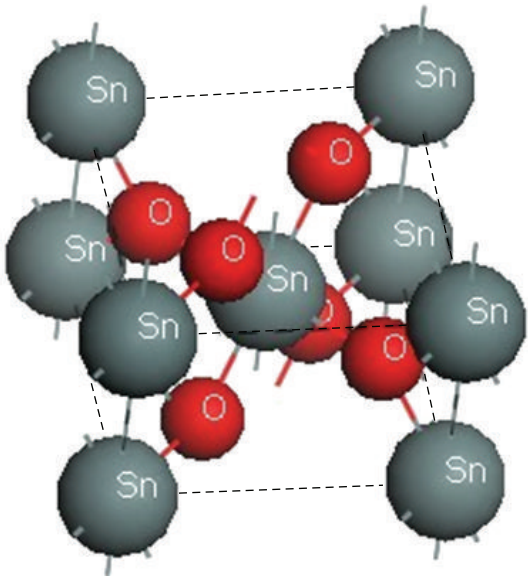

Figure 8: The unit cell model of rutile SnO_2.

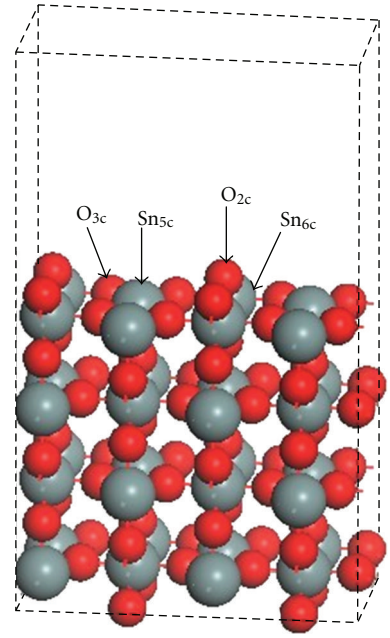

Figure 9: The atomic model of SnO_2 (110) surface.

SnO_2-based gas sensors, the first principles calculations were performed to investigate the interactions of H_2 and CO with SnO_2 (110) surface to reveal the sensing mechanism of SnO_2.

Firstly, we built the rutile SnO_2 unit cell model with lattice parameters $a = 4.737$ and $c = 3.186$ Å. As shown in Figure 8, each Sn atom is bonded with six O atoms nearby, and each O with three Sn. To preserve symmetry, the top and bottom layers of the slab were taken to be identical, and a surface vacuum slab of 10 Å was added to the (110) surface to avoid unnecessary interactions between the slabs. A super cell consisted of a 1×1 surface unit cell was employed, which was composed of a finite number of layers but of infinite extent. As shown in Figure 9, the SnO_2 (110) surface as a single slab consisted of several atomic layers, which was cut from the optimized bulk structure. The central five layers were constrained at their sites, while the surface and subsurface layers on either side of the slab were allowed to relax freely for all the calculations. There are four kinds of surface atoms: O_{2c}, O_{3c}, Sn_{5c}, and Sn_{6c}, respectively, as shown in Figure 9. The outermost atomic layer is composed of two coordinate oxygen anions O_{2c} (bridging oxygen), which occupy bridging positions between fully coordinated tin atoms Sn_{6c} located in the second layer. Five coordinated tin atoms Sn_{5c} (5-fold Sn^{4+}) and fully coordinated tin atoms Sn_{6c} (6-fold Sn^{4+}) as well as fully coordinated oxygen anions O_{3c} (plane oxygen) occupy the second layer. And the third atomic layer is constituted of subbridging oxygen atoms.

Table 1 listed the outermost atoms displacement of the rutile SnO_2 (110) surface with geometry optimization calculation by the CASTEP program module. The O_{2c}, O_{3c}, and Sn_{6c} atoms at the top layer move out of the surface by 0.04 Å, 0.16 Å, and 0.18 Å, respectively. While Sn_{5c} atom relaxes inwards 0.10 Å, which has the same tendency with the results reported in other literatures [23, 26, 32].

As mentioned above, the surface layer of SnO_2 (110) surface has four different characteristic atoms O_{2c}, O_{3c}, Sn_{5c}, and Sn_{6c}. Different from nonpolar molecules such as H_2, CO molecule is likely to be adsorbed on the surface layer atoms with its carbon end or oxygen end. In consideration of this, we initially imported CO gas molecule perpendicularly onto the surface layer atoms with carbon end to O_{2c} and O_{3c} sites and oxygen end to Sn_{5c} and Sn_{6c} sites, respectively. The initial vertical CO was placed at the sites that C atom could be bonded with Sn or O atom of SnO_2 (110) surface layer, and O atom could provide typical bond with Sn atom. Simultaneously, H_2 gas molecule was imported perpendicularly onto the surface layer atoms with the initial vertical heights that H atom could provide typical bond with surface layer atoms. The bond length and angle of adsorbed characteristic gas molecular models built in this work are in consistent with the theoretical data.

Table 1: Displacement of surface atoms along the (110) direction.

	O_{2c}	O_{3c}	Sn_{5c}	Sn_{6c}
DFT (GGA-RPBE)	0.04	0.16	−0.10	0.18
DFT (GGA-PBE) [32]	0.03	0.135	−0.092	0.15
DFT (GGA-PBE) [26]	0.09	0.18	−0.11	0.22
DFT (B3LYP) [23]	0.02	0.14	−0.12	0.26

In order to examine which adsorption position is the most energetically stable, we firstly calculated the adsorption energy (ΔE_{ads}) [18, 32, 44]. As a key parameter of the adhesive property of adsorption system, the adsorption energy is defined in the following equation [18, 32, 44]:

$$\Delta E_{ads} = E_{surf} + E_{gas} - E_{gas+surf}, \quad (2)$$

where E_{surf} is the energy of SnO_2 (110) surface before adsorption, E_{gas} is the energy of free gas molecule, and $E_{gas+surf}$ is the total energy of the system after adsorption. In general, a positive ΔE_{ads} indicates that the molecule adsorption process

Table 2: Adsorption energy on SnO_2 (110) surface.

	Adsorption energy ΔE_{ads}/eV			
Gas	O_{2c}	O_{3c}	Sn_{5c}	Sn_{6c}
H_2	0.031	0.018	0.024	0.027
CO (O end)			0.032	0.017
CO (C end)	0.021	0.029	0.042	0.024

is exothermic, and the adsorption system is energetically stable [18, 32]. For the purpose of comparison, all the energies are calculated with the supercell of identical size.

The calculated adsorption energies for detected gases adsorbed on SnO_2 (110) surface are represented in Table 2. According to the definition of adsorption energy, a positive value demonstrates an exothermic reaction, which means a stable adsorption process. The bigger the adsorption energy is, the greater the excitation chance of the gas molecule electrons is.

Table 2 shows that the ΔE_{ads} of hydrogen adsorbed on O_{2c} atom site is relatively higher than that of other adsorption sites, indicating that hydrogen adsorption on O_{2c} atom site is the most thermodynamically favored process. Therefore, it is considered as the most energetically stable adsorption geometry, and in our calculation results the corresponding ΔE_{ads} for hydrogen on O_{2c}, O_{3c}, Sn_{5c}, and Sn_{6c} is 0.031 eV, 0.018 eV, 0.024 eV, and 0.027 eV, respectively. Simultaneously, ΔE_{ads} for carbon monoxide with C end to O_{2c}, O_{3c}, Sn_{5c}, and Sn_{6c} is 0.021 eV, 0.029 eV, 0.042 eV, and 0.024 eV, respectively and O end to Sn_{5c} and Sn_{6c} is 0.032 eV, and 0.017 eV. The ΔE_{ads} of carbon monoxide with C end on Sn_{5c} (Sn_{6c}) atom site is somewhat higher than that with O end, meaning that carbon monoxide is favored to be adsorbed on Sn_{5c} (Sn_{6c}) atom site with C end. And the ΔE_{ads} of carbon monoxide with C end on Sn_{5c} atom site is relatively higher than that of other adsorption site; therefore, we can conclude that carbon monoxide adsorbed on SnO_2 (110) surface with C end on Sn_{5c} atom site is the most energetically stable adsorption position.

Further research on the difference of sensing properties can be performed by analyzing the total density of states (DOSs) and partial density of states (PDOSs) of gas molecule and atoms in the adsorption system. The DOSs and PDOS of O_{2c} and Sn_{5c} on SnO_2 (110) surface are demonstrated in Figure 10, the DOS of hydrogen and carbon monoxide before and after adsorption are shown in Figure 12. For a deeply understanding of the adsorption process, the DOS and PDOS of free CO molecule are also demonstrated in Figure 11.

From Figure 10, it can be seen that the lower valence band of O_{2c} is mainly contributed by the 2s orbits, and the upper valence band results from the 2p orbits. For Sn_{5c} atoms, the 5s and 5p orbits compose the valence band and conductance band together.

As seen in Figure 11, the DOS of free carbon monoxide is composed of 4σ, 1π, 5σ, and 2π orbits and the occupied 5σ orbit is at the Fermi level. The 4σ is mainly contributed by the 2p, 2s of O, and 2s of C, 1π mainly from the 2p of C and 2p of O, 5σ mainly from the 2s and 2p orbits of C, and 2π

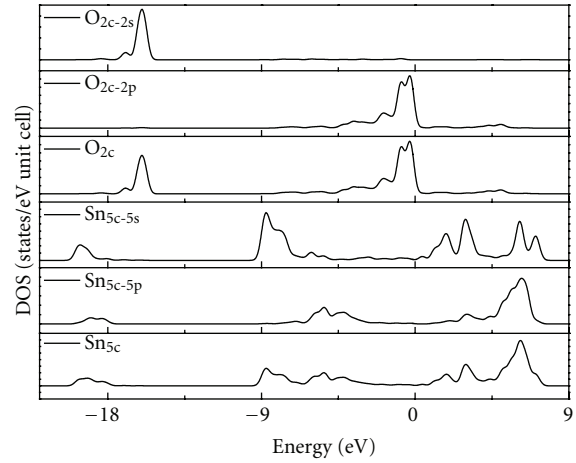

Figure 10: DOS and PDOS of O_{2c} and Sn_{5c} from SnO_2 (110) surface.

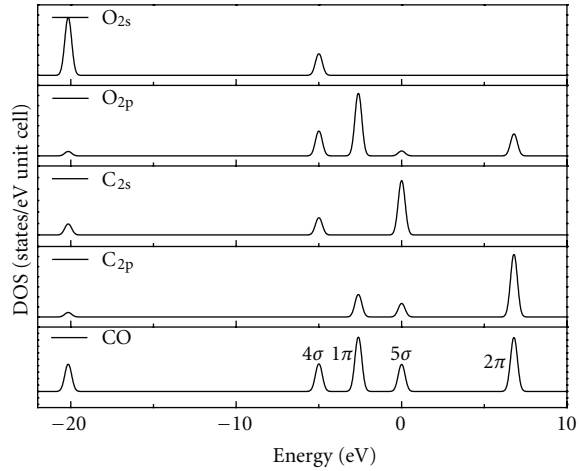

Figure 11: DOS and PDOS of free CO molecule.

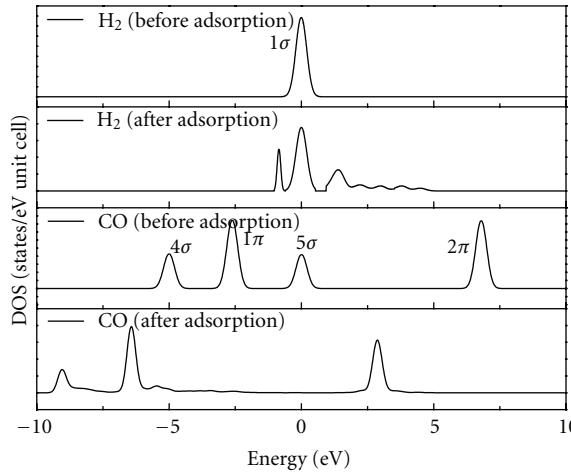

Figure 12: DOS of H_2 and CO before and after adsorption.

Table 3: The Mulliken charge and population of H_2 and CO.

		Before adsorption		After adsorption	
		s	p	s	p
H_2	H	0.62	0.03	0.60	0.01
	H	0.62	0.03	0.60	0.01
CO	C	1.68	1.90	1.51	2.16
	O	1.84	4.58	1.83	4.44

mainly from the 2p of C and 2p of O. After carbon monoxide adsorbed on Sn_{5c} site with C end on (110) surface, the DOS of adsorbed carbon monoxide decreases slightly and the 5σ orbits are almost completely degenerated. It implies a strong interaction between the 5σ orbits of CO molecule and 5s 5p orbits of Sn_{5c}.

For free hydrogen whose occupied 1σ orbital is at the Fermi level, the DOS of hydrogen changes slightly and obviously separates into several peaks after hydrogen adsorption on O_{2c} site. The change of DOS peaks indicates an interaction between the 1s orbital of adsorbed hydrogen and the 2p orbital of O_{2c} atoms, which may increase the probability of electron transfer from valence band to conductance band if intrinsic electrons are activated thermally or electronically.

The Mulliken population and charge transfer [18, 32, 44] between the gas molecule and adsorption surface was further investigated to illustrate the sensing mechanism of the rutile tin oxide to hydrogen and carbon monoxide. Table 3 demonstrates the Mulliken population of hydrogen and carbon monoxide before and after the adsorption on the (110) surface.

As shown in Table 3, the charge transfers of H_2 and CO gas molecule on (110) surface have the common tendency. The total number of electrons decreases at different degrees after being adsorbed on the surface. The number of the lost electrons from H_2 and CO is 0.08 e and 0.06 e, respectively. Accordingly, the lost electrons from adsorbed gas molecule are received by the (110) surface. It will decrease the height of barrier in the depletion region, increase the conductance of the sensor, and result in an increasing of output voltage which was generally observed in the on-line monitoring stage.

It should be noted that it is controversial to quantitatively interpret the gas sensing mechanism, due to the possible deviations between experimental conditions and ideal theoretical models. However, a qualitative comparison on different gas molecules adsorbed in the same adsorption system to investigate their different of sensing properties should be reliable [32].

4. Conclusions

This study has prepared nano-SnO_2 powder via hydrothermal method and investigated its morphology and microstructure. In particular, it focused on the gas sensing properties of the prepared sensor against power transformer fault gases such as hydrogen and carbon monoxide. Experiments showed that the optimum operating temperatures for 50 ul/L H_2 and CO were about 400°C and 360°C, with the gas response being 43.15 and 14.86, respectively.

Based on the first principles method the gas adsorption process was further investigated at the atomic level. Calculations results indicated that H_2 was favored to adsorb on O_{2C} site, and Sn_{5c} was the energetically stable adsorption position for CO with C end. After the adsorption of H_2 on O_{2C} site of (110) surface, there appeared new electronic peaks at the Fermi level. And the 5σ orbits of CO almost completely degenerated after CO adsorbed on Sn_{5c} position of (110) surface with C end. From the Mulliken population analysis, the lost electron number of H_2 and CO is 0.08 e and 0.06 e, respectively, and this will increase the conductance of the sensor.

The differences gas sensing properties of nano-SnO_2-based sensor towards H_2 and CO were qualitatively explained by the theoretical calculations. They will present a new feasible way on exploring new nano-SnO_2-based gas sensor and other sensing materials for on-line monitoring of fault gases dissolved in power transformers.

Acknowledgments

The authors acknowledge the support of the National Natural Science Foundation of China (51277185) and the Funds for Innovative Research Groups of China (51021005).

References

[1] H. Xiong, C. X. Sun, R. J. Liao, J. Li, and L. Du, "Study on kernel-based possibilistic clustering and dissolved gas analysis for fault diagnosis of power transformer," *Proceedings of the Chinese Society of Electrical Engineering*, vol. 25, no. 20, pp. 162–166, 2005.

[2] N. Y. Peng, X. S. Wen, Y. Wang, J. B. Chen, and X. Z. Chai, "Potential fault diagnosis method based on linear classifier for oil-immersed transformer," *Proceedings of the Chinese Society of Electrical Engineering*, vol. 24, no. 6, pp. 147–151, 2004.

[3] W. G. Chen, Y. X. Yun, C. Pan, and C. X. Sun, "Analysis of infrared absorption properties of dissolved gases in transformer oil," *Proceedings of the Chinese Society of Electrical Engineering*, vol. 28, no. 16, pp. 148–153, 2008.

[4] L. J. Zhou, G. N. Wu, P. Tang, H. L. Wang, and C. Su, "Model of semiconductor gas sensor for monitoring dissolved gases in insulation oil," *Automation of Electric Power Systems*, vol. 30, no. 10, pp. 75–79, 2006.

[5] A. Cirera, A. Cabot, A. Cornet, and J. R. Morante, "CO–CH_4 selectivity enhancement by in situ Pd-catalysed microwave SnO_2 nanoparticles for gas detectors using active filter," *Sensors and Actuators B*, vol. 78, no. 1–3, pp. 151–160, 2001.

[6] R. Ionescu, A. Vancu, C. Moise, and A. Tomescu, "Role of water vapour in the interaction of SnO_2 gas sensors with CO and CH_4," *Sensors and Actuators B*, vol. 61, no. 1, pp. 39–42, 1999.

[7] Y. Shimizu, T. Maekawa, Y. Nakamura, and M. Egashira, "Effects of gas diffusivity and reactivity on sensing properties of thick film SnO_2-based sensors," *Sensors and Actuators B*, vol. B46, no. 3, pp. 163–168, 1998.

[8] S. D. Choi and D. D. Lee, "CH_4 sensing characteristics of K-, Ca-, Mg impregnated SnO_2 sensors," *Sensors and Actuators B*, vol. 77, no. 1-2, pp. 335–338, 2001.

[9] J. Huang, N. Matsunaga, K. Shimanoe, N. Yamazoe, and T. Kunitake, "Nanotubular SnO_2 templated by cellulose fibers: synthesis and gas sensing," *Chemistry of Materials*, vol. 17, no. 13, pp. 3513–3518, 2005.

[10] M. R. Cássia-Santos, V. C. Sousa, M. M. Oliveira et al., "Recent research developments in SnO_2-based varistors," *Materials Chemistry and Physics*, vol. 90, no. 1, pp. 1–9, 2005.

[11] M. E. Franke, T. J. Koplin, and U. Simon, "Metal and metal oxide nanoparticles in chemiresistors: does the nanoscale matter?" *Small*, vol. 2, no. 1, pp. 36–50, 2006.

[12] M. Sauvan and C. Pijolat, "Selectivity improvement of SnO_2 films by superficial metallic films," *Sensors and Actuators B*, vol. 58, no. 1–3, pp. 295–301, 1999.

[13] R. M. Prasad, A. Gurlo, R. Riedel, M. Hübner, N. Barsan, and U. Weimar, "Microporous ceramic coated SnO_2 sensors for hydrogen and carbon monoxide sensing in harsh reducing conditions," *Sensors and Actuators B*, vol. 149, no. 1, pp. 105–109, 2010.

[14] A. Köck, A. Tischner, T. Maier et al., "Atmospheric pressure fabrication of SnO_2-nanowires for highly sensitive CO and CH_4 detection," *Sensors and Actuators B*, vol. 138, no. 1, pp. 160–167, 2009.

[15] T. Zhang, L. Liu, Q. Qi, S. Li, and G. Lu, "Development of microstructure In/Pd-doped SnO_2 sensor for low-level CO detection," *Sensors and Actuators B*, vol. 139, no. 2, pp. 287–291, 2009.

[16] Q. Qi, T. Zhang, X. Zheng et al., "Electrical response of Sm_2O_3-doped SnO_2 to C_2H_2 and effect of humidity interference," *Sensors and Actuators B*, vol. 134, no. 1, pp. 36–42, 2008.

[17] F. Quaranta, R. Rella, P. Siciliano et al., "Novel gas sensor based on SnO_2/Os thin film for the detection of methane at low temperature," *Sensors and Actuators B*, vol. 58, no. 1–, pp. 350–355, 1999.

[18] W. Zeng, T. M. Liu, D. J. Liu, and E. J. Han, "Hydrogen sensing and mechanism of M-doped SnO_2 (M = Cr^{3+}, Cu^{2+} and Pd^{2+}) nanocomposite," *Sensors and Actuators B*, vol. 160, no. 1, pp. 455–462, 2011.

[19] C. W. Zhang, P. J. Wang, and F. Li, "First-principles study on surface magnetism in Co-doped (110) SnO_2 thin film," *Solid State Sciences*, vol. 13, no. 8, pp. 1608–1611, 2011.

[20] M. Hübner, R. G. Pavelko, N. Barsan, and U. Weimar, "Influence of oxygen backgrounds on hydrogen sensing with SnO_2 nanomaterials," *Sensors and Actuators B*, vol. 154, no. 2, pp. 264–269, 2011.

[21] H. Zhang, Z. Li, L. Liu et al., "Enhancement of hydrogen monitoring properties based on Pd-SnO_2 composite nanofibers," *Sensors and Actuators B*, vol. 147, no. 1, pp. 111–115, 2010.

[22] Y. Wang, Q. Mu, G. Wang, and Z. Zhou, "Sensing characterization to NH_3 of nanocrystalline Sb-doped SnO_2 synthesized by a nonaqueous sol-gel route," *Sensors and Actuators B*, vol. 145, no. 2, pp. 847–853, 2010.

[23] J. Oviedo and M. J. Gillan, "Energetics and structure of stoichiometric SnO_2 surfaces studied by first-principles calculations," *Surface Science*, vol. 463, no. 2, pp. 93–101, 2000.

[24] J. B. L. Martins, E. Longo, J. Andrés, and C. A. Taft, "Theoretical study of cluster models and molecular hydrogen interaction with SnO_2 [110] surface," *Journal of Molecular Structure: THEOCHEM*, vol. 335, no. 1–3, pp. 167–174, 1995.

[25] M. Calatayud, J. Andrés, and A. Beltrán, "Theoretical analysis of adsorption and dissociation of CH_3OH on the stoichiometric SnO_2(110) surface," *Surface Science*, vol. 430, no. 1, pp. 213–222, 1999.

[26] J. Oviedo and M. J. Gillan, "First-principles study of the interaction of oxygen with the SnO_2 (110) surface," *Surface Science*, vol. 490, no. 3, pp. 221–236, 2001.

[27] J. Oviedo and M. J. Gillan, "Reconstructions of strongly reduced SnO_2 (110) studied by first-principles methods," *Surface Science*, vol. 513, no. 1, pp. 26–36, 2002.

[28] F. Ciriaco, L. Cassidei, M. Cacciatore, and G. Petrella, "First principle study of processes modifying the conductivity of substoichiometric SnO_2 based materials upon adsorption of CO from atmosphere," *Chemical Physics*, vol. 303, no. 1-2, pp. 55–61, 2004.

[29] M. A. Mäki-Jaskari, T. T. Rantala, and V. V. Golovanov, "Computational study of charge accumulation at SnO_2 (110) surface," *Surface Science*, vol. 577, no. 2-3, pp. 127–138, 2005.

[30] C. W. Zhang, P. J. Wang, and F. Li, "First-principles study on surface magnetism in Co-doped (110) SnO_2 thin film," *Solid State Sciences*, vol. 13, no. 8, pp. 1608–1611, 2011.

[31] T. T. Rantala, T. S. Rantala, and V. Lantto, "Electronic structure of SnO_2 (110) surface," *Materials Science in Semiconductor Processing*, vol. 3, no. 1-2, pp. 103–107, 2000.

[32] Z. Wen, L. Tian-Mo, and L. Xiao-Fei, "Hydrogen sensing properties of low-index surfaces of SnO_2 from first-principles," *Physica B*, vol. 405, no. 16, pp. 3458–3462, 2010.

[33] V. N. Mishra and R. P. Agarwal, "Sensitivity, response and recovery time of SnO_2 based thick-film sensor array for H_2, CO, CH_4 and LPG," *Microelectronics Journal*, vol. 29, no. 11, pp. 861–874, 1998.

[34] N. Yamazoe, G. Sakai, and K. Shimanoe, "Oxide semiconductor gas sensors," *Catalysis Surveys from Asia*, vol. 7, no. 1, pp. 63–75, 2003.

[35] I. J. Kim, S. D. Han, I. Singh, H. D. Lee, and J. S. Wang, "Sensitivity enhancement for CO gas detection using a SnO_2-CeO_2-PdO_x system," *Sensors and Actuators B*, vol. 107, no. 2, pp. 825–830, 2005.

[36] H. Lu, W. Ma, J. Gao, and J. Li, "Diffusion-reaction theory for conductance response in metal oxide gas sensing thin films," *Sensors and Actuators B*, vol. 66, no. 1–3, pp. 228–231, 2000.

[37] Y. Shen, T. Yamazaki, Z. Liu, D. Meng, and T. Kikuta, "Hydrogen sensors made of undoped and Pt-doped SnO_2 nanowires," *Journal of Alloys and Compounds*, vol. 488, no. 1, pp. L21–L25, 2009.

[38] B. Wang, L. F. Zhu, Y. H. Yang, N. S. Xu, and G. W. Yang, "Fabrication of a SnO_2 nanowire gas sensor and sensor performance for hydrogen," *Journal of Physical Chemistry C*, vol. 112, no. 17, pp. 6643–6647, 2008.

[39] A. Srivastava and K. Jain, "Study on ZnO-doped tin oxide thick film gas sensors," *Materials Chemistry and Physics*, vol. 105, no. 2-3, pp. 385–390, 2007.

[40] Y. B. Xue and Z. A. Tang, "Density functional study of the interaction of CO with undoped and Pd doped SnO_2 (110) surface," *Sensors and Actuators B*, vol. 138, no. 1, pp. 108–112, 2009.

[41] G. Wu, J. Zhang, Y. Wu, Q. Li, K. Chou, and X. Bao, "Adsorption and dissociation of hydrogen on MgO surface: a first-principles study," *Journal of Alloys and Compounds*, vol. 480, no. 2, pp. 788–793, 2009.

[42] F. Trani, M. Causà, D. Ninno, G. Cantele, and V. Barone, "Density functional study of oxygen vacancies at the SnO_2 surface and subsurface sites," *Physical Review B*, vol. 77, no. 24, Article ID 245410, pp. 245–252, 2008.

[43] Y. C. Lee, H. Huang, O. K. Tan, and M. S. Tse, "Semiconductor gas sensor based on Pd-doped SnO_2 nanorod thin films," *Sensors and Actuators B*, vol. 132, no. 1, pp. 239–242, 2008.

[44] J. D. Prades, A. Cirera, J. R. Morante, J. M. Pruneda, and P. Ordejón, "Ab initio study of NOx compounds adsorption on SnO_2 surface," *Sensors and Actuators B*, vol. 126, no. 1, pp. 62–67, 2007.